Physical properties of Hradište border fault (Turiec Basin, Western Carpathians, Slovakia) inferred by multidisciplinary geophysical approach

DAVID KUŠNIRÁK[1], HERMANN ZEYEN[2], MIROSLAV BIELIK[1,3,✉], RENÉ PUTIŠKA[1],
ANDREJ MOJZEŠ[1], BIBIANA BRIXOVÁ[1], ROMAN PAŠTEKA[1], IVAN DOSTÁL[1],
PAVOL ZAHOREC[3], JURAJ PAPČO[4], JOZEF HÓK[5], MARIÁN BOŠANSKÝ[1]
and MARTIN KRAJŇÁK[1]

[1]Department of Applied and Environmental Geophysics, Faculty of Natural Sciences, Comenius University, Mlynská dolina, Ilkovičova 6,
842 15 Bratislava, Slovakia; ✉bielik1@uniba.sk
[2]Département des Sciences de la Terre, UMR 8146, Université de Paris-Saclay, CNRS, Orsay, France
[3]Earth Science Institute of the SAS, the Slovak Academy of Sciences, Dúbravská cesta 9, 840 05 Bratislava, Slovakia
[4]Department of Theoretical Geodesy, Faculty of Civil Engineering, STU in Bratislava, Radlinského 11, 810 05 Bratislava, Slovakia
[5]Department of Geology and Paleontology, Faculty of Natural Sciences, Comenius University, Mlynská dolina, Ilkovičova 6,
842 15 Bratislava, Slovakia

Abstract: The Hradište border fault zone has played an important role in the development of the tectonic contact of the Cenozoic sediments of the Turiec Basin with the Malá Fatra Mountains crystalline basement. Seismic, geoelectric, radiometric, gravimetric, magnetometric and ground penetrating radar measurements were used to study the physical properties and determine the exact position and inclination of this fault zone down to a depth of up to 40 m. The Hradište border fault zone represents an almost vertical physical boundary characterized by decreasing seismic velocity (from 3.0 km.s^{-1} to 2.2 km.s^{-1}) and decreasing electrical resistivity (500 to 150 Ω.m) when passing from the basement west of the fault to sediments to its east. It corresponds also to a compact segment of the lowest volume activity of radon ^{222}Rn values in soil air (8 kBq.m^{-3} on average) and maximum horizontal gravity gradient (−0.0076 mGal.m^{-1}). The discovery of this anomalous zone also helps us to distinguish two different anomalous blocks. The block west of the fault represents the orthogneisses of the Tatric crystalline complex belonging to the Malá Fatra Mountains. The eastern block is built-up by the Bystrička Member Pliocene sediments of the Turiec Basin. Our study serves as a case study for geophysical research on faults in different tectonic units of the Western Carpathians and other similar orogens.

Keywords: Near-surface geophysics, seismic tomography, electrical resistivity tomography, ground-penetrating radar, self-potential, radiometry, gravimetry, magnetometry, border fault, Turiec Basin, Western Carpathians.

Introduction

Basins, grabens and intramountain depressions are typical morphotectonic features of the Western Carpathians. Tectonic evolution of basins and depressions is connected with the geodynamic processes which controlled the development of the Carpathian arc during the Neogene. Recent structural arrangement is the result of the back-arc extension regime operated from the Middle Miocene and most probably persisted until the Quaternary (Kováč et al. 2011). Normal faults, often with considerable offsets, were predominantly activated along the future margins of depressions. Especially intermontane depressions, such as the Turiec Basin, were filled with detritic material eroded from the uplifting mountains and mostly reflecting composition of the source areas.

The Turiec Basin (Fig. 1) has a half-graben type structure with sedimentary fill dipping generally towards the West. This fact points to the tectonic activity of the border fault (the Hradište border fault) situated on western basin margin (e.g.,

Kilényi & Šefara 1989; Šefara et al. 1987; Nemčok & Lexa 1990; Hók et al. 1998) being the largest. The assumed NNE–SSW strike of the Hradište fault zone would follow the Lúčanská Malá Fatra mountain front. It should delimit massive landforms such as faceted slopes and flattened surfaces. The fact that this mountain front was not destroyed by exogenic processes strengthens the hypothesis of active tectonics during the Quaternary (Vojtko et al. 2011). The landforms are the results of rapid exhumation (from Upper Miocene to Present) of the Lučanská Malá Fatra Mts. and subsidence along the western margin of the Turiec Basin. A remarkable mosaic of landforms (Kováč et al. 2011) has been discovered at the front of the faceted slope line of the Hradište fault zone with many alluvial fans of different areal extent and volume. The Pliocene to Holocene alluvial fans were deposited by gravity flows and stream sedimentation and their presence in the eastern part of the Kriváňska Malá Fatra mountain front line is a result of sudden change in slope. Knickpoints in river longitudinal profiles (mainly

in the foothills of the Malá Fatra Mts. (Sládek 2010) indicate recent tectonic activity. Quaternary tectonic activity is also most likely a cause of block landslides in some parts of the boundary between the mountains and the Turiec Basin.

Just these landslides and widespread presence of Quaternary cover at the surface makes direct observation of these border faults impossible. Therefore our research was focused on the geophysical study of the significant Hradište border fault, which played important role in evolution of the Turiec Basin and the Lúčanská Malá Fatra Mts.

The Hradište border fault is a contact between the Lúčanská Malá Fatra Mts. (in the West) and the Turiec Basin (in the East). The two tectonic units are composed of completely different rocks. The Lúčanská Malá Fatra Mts. is composed of the Tatric crystalline complex, while the Turiec Basin is filled with Neogene sediments. As the composition of these units is completely different it can be assumed that they are also characterized by different physical properties. This assumption is strongly supported by the results of Panáček et al. (1991). Taking this into account we expect that the physical parameters of the rocks of both tectonic units will differ in seismic velocity, resistivity, magnetic susceptibility, density, radioactivity and soil grain size.

That is why we have used a wide spectrum of geophysical methods, including seismic tomography, electrical-resistivity tomography (ERT), electromagnetic induction (EMI), ground-penetrating radar (GPR), self-potential (SP), radiometry, gravimetry and magnetometry for accurate mapping of the Hradište border fault and its imaging in depth. The common use of these methods aims at increasing the reliability of geological interpretation and may help to reduce uncertainties or non-unicity of the interpretation of certain methods. Additionally, it gives an overview of the capability of the different methods to image similar border faults of the Western Carpathian intramountain depressions.

Geological settings

The Turiec Basin is the northernmost intramountain Cenozoic depression of the Western Carpathians in Slovakia (Fig. 1). This basin is unique in that it has been completely isolated from other basins during the whole Neogene (Upper Miocene) development. It is about 40 km long and 10 km wide and elongated in a NNE–SSW direction.

The western flank of the basin is part of the Lúčanská Malá Fatra Mountains, while the eastern flank borders the Veľká Fatra Mountains. Both are composed of the Mesozoic complexes of the Fatric or Hronic superficial nappes and the Hercynian crystalline complex of the Tatric thick-skinned unit (Hók et al. 1998; Kováč et al. 2011). The northern margin of the basin is formed by the Kriváňska Malá Fatra Mountains, which are predominantly composed of the Hercynian crystalline basement of the Tatric Unit. The Tatric crystalline basement of the Žiar Mountains and the volcano-sedimentary complex of the Kremnické Vrchy Mountains restrict the basin to the south.

The Turiec Basin is predominantly filled with Upper Miocene to Pliocene sediments with negligible occurrence of the Middle and Lower Miocene deposits in the south.

The pre-Neogene basement of the basin consists of paleo-Alpine allochthonous Mesozoic complexes and a Paleogene post-nappe sedimentary cover in its northern part (Fusán et al. 1987; Fendek et al. 1990; Kováč et al. 2011; Bielik et al. 2013).
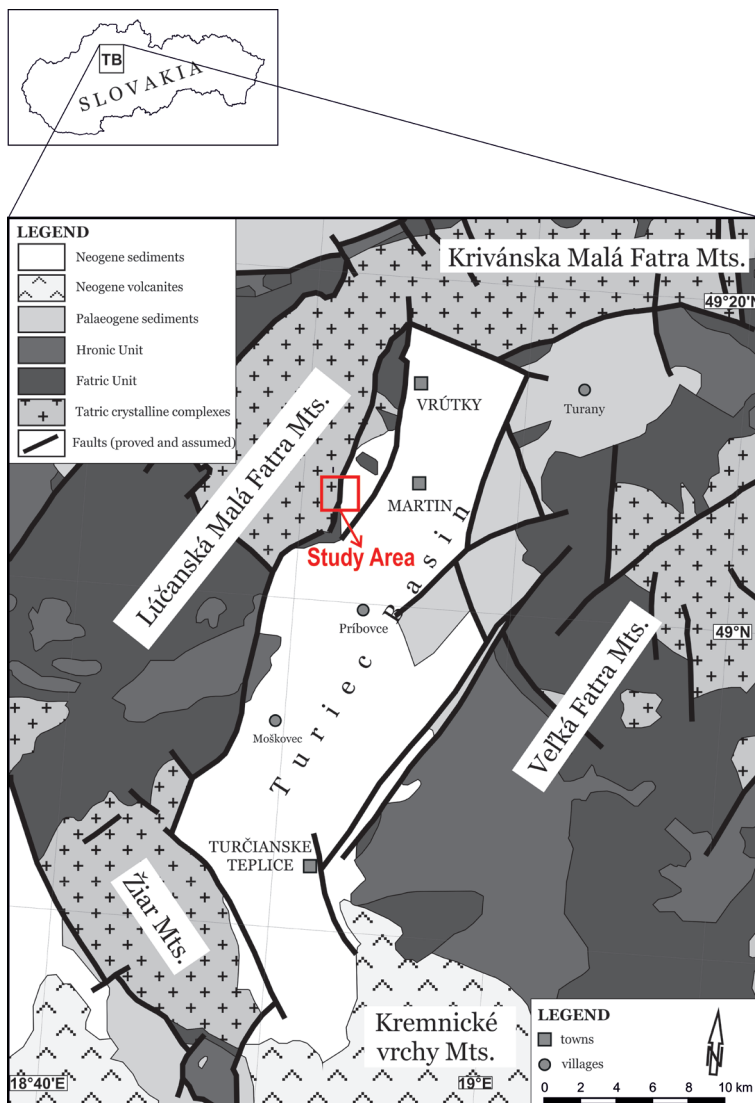

Fig. 1. Simplified geological map of the Turiec Basin and its surroundings. The study area is highlighted by the red rectangle (after Kováč et al. 2011 and Bielik et al. 2013).

Applied geophysical methods

Application of shallow subsurface geophysical imaging of fault zones is a powerful tool. Seismic and geoelectrical methods are most popular as they can provide high-resolution tomographic images of the fault zone (among others: Sheley et al. 2003; Villani et al. 2015; Pucci et al. 2016), also magnetic and gravity surveys are commonly employed for locating faults (Linsser 1967; Klinger et al. 2016). Employment of ground penetrating radar or radiometric methods are also applicable, but less established, since they provide very shallow information only and can be significantly influenced or attenuated by a sedimentary cover (Slater & Niemi 2003; Dubey et al. 2012). In optimal conditions many studies pointed out that soil gas methods, mainly radon emanometry, are reliable investigation tools in neotectonic studies and for mapping of fault zones (Guerra & Lombardi 2001; Singh et al. 2006; Giammanco et al. 2009).

The 440 m long profile A–A' is located at the junction of Lúčanská Fatra Mts. and Turiec Basin and extends almost perpendicular to the Hradište fault (Fig. 2), which separates these two tectonic units. From a geological point of view, this fault forms the boundary between the crystalline basement of the Tatric Unit in Lúčanská Fatra Mts. and the Neogene sediments (the Bystrička Member after Kováč et al. 2011) of theTuriec Basin.

Spatial coordinates of the profile points were determined using GNSS measurements in Real Time Kinematic (RTK) mode and by spatial polar methods using terrestrial geodetic measurements (horizontal and vertical angles and spatial distances). RTK measurements were realized using the Slovak official positioning service SKPOS in Virtual Reference Station (VRS) concept with a Trimble R8 GNSS receiver. Terrestrial measurements were realized using automatic total stations Trimble S8. Final coordinates were computed with the Trimble Business Centre (v. 2.2) software. Global horizontal accuracy of the points was better than ±0.020 m and vertical accuracy was better than ±0.025 m. The resulting coordinates of the first and final points of profile A–A' are 49°03'27.7"N, 18°50'46.57"E and 49°03'19.91"N, 18°51'4.12"E. Additional 850 topographical points were measured in the area for a better resolution of the local digital terrain model anomalies in computation of the gravity terrain effect.

The *seismic line* was acquired with a DMT-Summit 40 channel equipment, a hammer as source with 4 to 10 stacks and 10 Hz geophones. The geophones were deployed every 2 m and the source points were separated by 4 m. The data were thus acquired in blocks of 80 m length with fixed geophone position and moving source points. After the acquisition of one block, half of the geophones were shifted behind the end of the block and the source went back to the beginning of the new deployment. In this way, the 440 m long line was acquired in ten overlapping blocks. Some 6000 P-wave travel times were picked, and a joint model was prepared using the forward modelling (trial and error) ray-tracing algorithm of Zelt & Smith (1992), taking into account the topography.

The *2D ERT (Electrical resistivity tomography) line* was collected using an ARES instrument (GF Instruments Inc.). The survey was 435 m long using a Wenner alpha array configuration with 5 m electrode spacing. In total 88 electrodes were used simultaneously. For post-processing and data interpretation, the inversion program RES2DINV (Loke & Barker 1996) was applied. It generates a topographically corrected 2D resistivity model of the subsurface by inverting the apparent resistivity data. Robust inversion (L1 norm) was used because it is more suitable for detecting sharp linear features such as faults.

The *EMI (Electromagnetic interference) data* was collected using a CMD-Explorer instrument (GF Instruments Inc.). The CMD-Explorer is a multi-receiver coil, electromagnetic conductivity instrument with receiver coils at 1.48 m, 2.82 m and 4.49 m from the transmitter, in vertical dipole mode, which equates to effective depth penetrations of 2.3 m, 4.2 m and 6.7 m respectively. The survey was 435 m long, the data were collected in manual mode, a point every 1m. EMI data have been interpreted using EM4Soil, a software package developed to enable the inversion of EMI apparent conductivity (σ_a) data acquired at low induction numbers (EMTOMO 2015). Forward modelling of the EM4Soil software is based on the cumulative function (McNeill 1980) or on the full solution of EM fields in a layered Earth (Keller & Frischknecht 1996). The inversion algorithm based on the Occam regularization method (Sasaki 1989, 2001) was described and applied in several other studies (Triantafilis et al. 2003; Monteiro Santos et al. 2010; Triantafilis & Monteiro Santos 2013).

The *gravity data* were acquired along the profile at 89 points with a point separation of 5 m by means of a Scintrex CG-5 gravity meter. During the measurements, a base-point was repeated every 1–2 hours with the aim of proper sampling of the instrumental drift. Before the profile measurements, the base point was tied to the State Gravity Network in the Gravity-System-1995. The gravity measurement uncertainty was estimated based on repeated profile points to about ±5 μGal.

Drift-corrected gravity values, heights and coordinates of measured points were processed into the form of complete Bouguer anomalies (CBA) by standard procedure based on the formula:
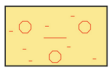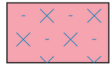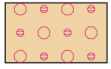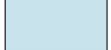
$$\text{CBA} = g - \gamma_0 - g_{FA} - \delta g_{TSL} + \delta g_{atm} + T,$$

where g is the drift-corrected gravity value, γ_0 is the normal gravity, δg_{FA} is free-air correction, δg_{TSL} is gravity effect of truncated spherical layer up to 166.7 km, δg_{atm} is atmospheric correction and T is terrain correction evaluated up to a distance of 166.7 km.

The sum of the second and third terms in the CBA defining equation constitutes the normal gravity at the observation point (Vajda & Pánisová 2005). The innermost zone terrain corrections were estimated using in situ geodetic measurements. For CBA calculation, a density of 2670 kg.m^{-3} was used, which corresponds to the density of the orthogneisses of
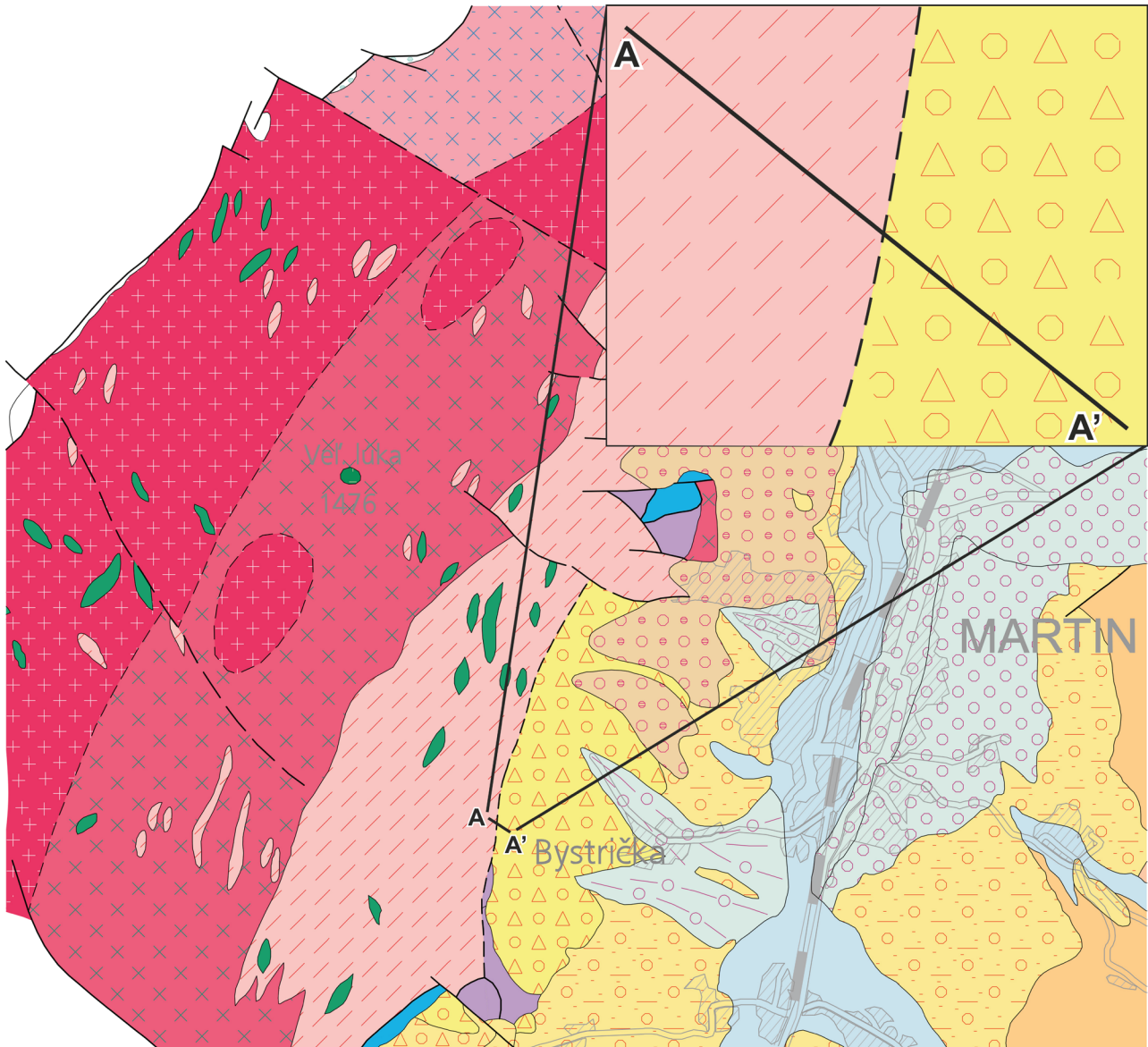
Legend

Tonalite - Granodiorite

Granodiorite

Granodiorite - Granite

Orthogneisses

Amphibolite

Mesozoic carbonates

Bystrička Member

Martin formation

Podstráne Member

Clays

Proluvial fan

Fluvial sediments
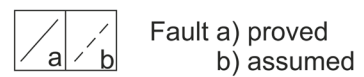
Fault a) proved
b) assumed

Fig. 2. Location of the investigated Profile A–A' on a detailed geological map (after Polák et al. 2008). Coordinates of the first and final points of the profile are A: 49°03'27.7''N; 18°50'46.57''E and A': 49°03'19.91'' N; 18°51'4.12''E.

the basement on the western side of the fault zone. For the interpretation of the data, we used rock densities obtained from laboratory analysis of the involved geological formations (Panáček et al. 1991), namely 2670 kg.m^{-3} for the orthogneisses of the Tatric crystalline complex in the NW part of the profile and 2560 kg.m^{-3} for the sedimentary fill of the TB.

The *SP (Self potential)* is the naturally occurring electrical potential of the Earth resulting from geological, geochemical, and hydrological interactions (Corry et al. 1983). Even though the data could be slightly affected by topography and by seasonal changes in soil and pore water resistivity, negative SP anomalies are often associated with subsurface down-going water flow paths and positive SP anomalies are associated with areas of outflow. The self-potential method was applied in the fixed-base configuration with non-polarizable electrodes (Cu/CuSO$_4$). The step of measurements was equal to 5 m and the measured values were corrected by the value of polarization of the electrodes before and after measurement.

Radiometric methods are sometimes very useful for detailed study of a fault and its geological surroundings. Mainly soil radon (^{222}Rn) emanometry may give valuable information about gas permeability of faulted rocks and, together with gamma-ray spectrometry, it can help to find boundaries between different lithological units. ^{222}Rn being a gaseous element, soil radon emanometry is an atmo-geochemical survey method based on measuring alpha activity in soil air samples from different depths of rock, weathering cover and soil. This activity results from alpha disintegration processes in the nuclei of radon isotope ^{222}Rn and its daughter products. Its parent radium isotope ^{226}Ra commonly occurs in basement rocks. A fault system is a very appropriate structure for upward movement of radon and other gases emanating from the interior of the Earth. Therefore, volume activity of the radon gas in the soil along the profile crossing the assumed fault zone, measured in kBq.m^{-3}, may contribute to its positioning. Radon measurements were performed on samples from approximately 0.8 m depth by a portable radon detector LUK-3R (SMM, CZ). In total, 32 stations were measured along the same profile with a 10 to 20 m step between measurements. A profile survey using ground gamma-ray spectrometry was used to study the radioactivity of rocks, soils and covers. This method allowed us to determine four measures of gamma-ray activity of near-surface rock and soil horizon at each measured station: total gamma-ray activity eUt [Ur] (Ur is a unit of radioelement concentration, 1 Ur≈1 ppm eU), concentration of ^{40}K [% K], concentration of ^{238}U [ppm eU], and concentration of ^{232}Th [ppm eTh], where the letter ''e'' represents "equivalent". The depth range is relatively shallow, no more than 1 m from the surface, but the method gives useful information mainly for spatial distribution of radioactive elements contained in geological units. In situ measurements were carried out using a portable 256-channel gamma-ray spectrometer GS-256 (Geofyzika, Czechoslovakia) with 3''×3'' NaI (Tl) scintillation detector using a traditional ground survey procedure: grass, old leaves, and the thin uppermost humus soil layer were removed, and ground surface was levelled in

a circular area of 1 to 1.5 m in diameter at each measured station. Time of measurement was 2 minutes per station. In total, 45 stations were measured along the profile with a 10-m step between measurements.

For a more objective interpretation, laboratory analysis of soil grain size was performed to evaluate the fraction of fine-grained clay particles in a sample. Eight soil samples were taken from depths up to 1 metre along the measured line. Soil permeability categories were determined based on the ratio between grain diameters below and above 0.063 mm, using the Slovak Technical Norm STN 72 1001 (2010) (Soil and rock classification).

The *GPR (Ground-penetrating radar)* detects electrical discontinuities in the shallow subsurface (typically <10 m depth) by generating and recording discrete pulses of high-frequency electromagnetic waves, reflected at layer boundaries (Neal 2004). The GPR used in this study was a GSSI SIR3000 unit equipped with a shielded 100 MHz antenna. The data were collected along the profile in a point mode with reading separation of 1 m along the profile. Every reading consisted of 100 stacked measurements in order to increase the signal-to-noise ratio. The total length of the measured section was 440 m. For GPR data processing and visualization Reflex-W software version 7.5 (Sandmeier 2014) was used, where the processing comprised the following basic steps: (a) removal of the direct wave (de-wow) by subtracting the mean value within a time range from each recorded trace, (b) adjusting the start time to the actual direct-wave onset on each trace, (c) bandpass filtering in order to improve the signal-to-noise ratio, (d) gain adjustment to recover the signal attenuation with depth, (e) background removal was applied to remove horizontal stripe noise from the dataset and (f) topography migration and static corrections were used for topography corrections.

Finally, *geomagnetic* data have been acquired around the profile along 3 parallel lines with a single sensor Caesium-vapour magnetometer TM-4, with a line separation of 1 m and a sampling step of 0.2 m. An internal odometer has been used to ensure precise sampling along the profile. Acquired Total Magnetic Intensity (TMI) data have been processed into anomalous magnetic field – diurnal variations and normal field removal have been realized by means of median filter application in a moving window with a length of 20 m.

Results

The seismic tomography (Fig. 3) shows at the top a thin layer with velocities of less than 0.3 km.s^{-1}, interpreted as soil and a 5 to 10 m thick layer with velocities of 1 to 1.5 km.s^{-1} interpreted as the non-saturated zone above the water table. Underneath these superficial layers, a clear approximately vertical boundary is visible at 165 m along the profile. This boundary separates two different geological environments. The area located to the NW of the boundary is characterized by higher P-wave velocities (on average >3.5 km.s^{-1}) and corresponds to the crystalline rocks, whereas to the SE,
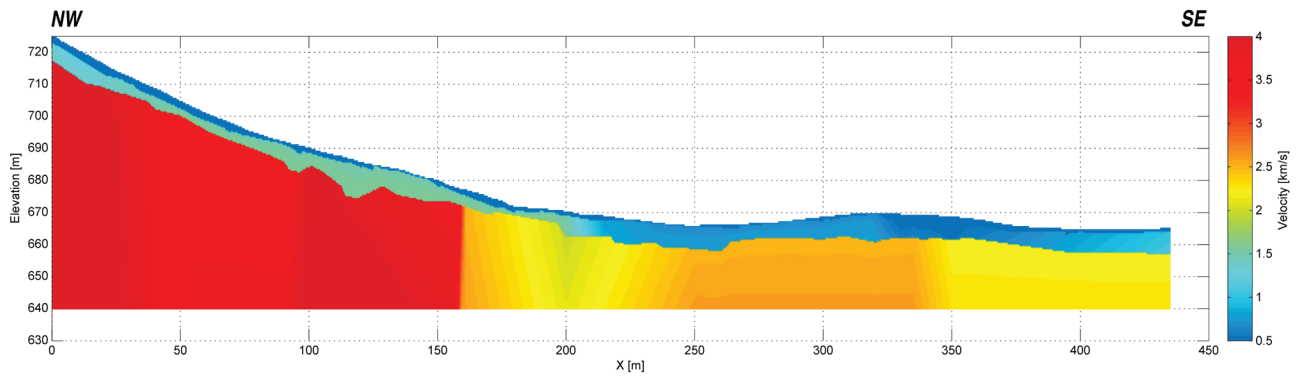
Fig. 3. P-wave velocity cross-section along the Profile A–A' constructed from seismic tomography measurement. A clear boundary is visible at approximately 165 m from the origin of profile representing the Hradište fault. Tatric crystalline rocks with higher P-wave velocities (>3.5 km.s^{-1}) to the NW of the fault are separated from the SE block with lower velocities (2.0–2.5 km.s^{-1}) corresponding to the Neogene sediments.

the Neogene sedimentary rocks have lower velocities (2.0–2.5 km.s^{-1}). The velocities in the non-saturated layer are also higher above the crystalline rocks than above the sediments. These higher velocities spread some 40 m further downhill than the limit detected at depth. This can be interpreted by downhill transport of weathered basement material.

Figure 4a displays the results of the resistivity inversion along the Profile A–A' based on 1146 measurement points with 0.11 % measurement uncertainty, the adjustment misfit being 2.5 % after seven iterations. In this cross section, the resistivity values range between 50 Ω.m and about 700 Ω.m and a significant vertical contrast between two blocks can be seen at the same position as in the seismic section. The NW block represented by the Tatric crystalline rocks is characterized by higher resistivity values (>400 Ω.m), while in the SE block, the resistivity of the Neogene sediments is smaller (<200 Ω.m). The resistivity contrast between the crystalline complex and Neogene sediments is detected at approximately 165 m from the origin of the profile. Based on the electrical resistivity tomography results, it can be concluded that the interpreted fault is almost vertical. Similar to the seismic profile, the resistivity profile shows a high-resistivity zone near the surface some 30 m further downhill than the limit at depth, reinforcing the hypothesis of basement rocks having slid downhill.

Figure 4b shows a contour plot of the 2D model of resistivity obtained by EMI measurements. It confirms the ERT results in the uppermost 7 m with largest values (>350 Ω.m) in the NW representing the Tatric crystalline rocks and smaller values (<200 Ω.m) in the SE for the Neogene sediments, without, however, showing the high-resistivity zone near the surface SE of the fault zone.

Taking into account the results of all the above-mentioned geophysical methods, a simple 2D density model was constructed (Fig. 5). This simple model consists of two blocks with different densities, which are separated by the interpreted Hradište fault. The NW block has a density of 2670 kg.m^{-3}, corresponding to that of orthogneiss rocks forming the Tatric crystalline complex of the Lúčanská Fatra Mts. The rocks of

the Bystrička Member SE of the fault, which belong to the sedimentary fill of the TB, have an average density of 2560 kg.m^{-3}. It is worth noting that the difference between the measured maximum (above orthogneisses) and minimum (above Bystrička Member) values of gravity is very small, only 1.75 mGal. The best fit between measured and calculated gravity values was obtained for a location of the Hradište fault at 165 m.

The basic trend of the SP field (Fig. 6) is increasing in the slope direction, which reflects the groundwater movement in the Quaternary sediments down the slope. In this trend there are local anomalies of increased values of electric potential, caused by the occurrence of clay accumulations (also confirmed by changes of clay content in the samples presented in Fig. 6) creating barriers to groundwater movement (metres 65 m and 125 m). On the other hand the increased values of SP observed between 310–360 m are due to rocky material [supported by the results of ERT (Fig. 4) and Georadar (Fig. 7)], which causes leakage of groundwater to deeper levels. The tectonics (the Hradište fault) interpreted at 165 m do not show any results significantly in the SP field measurement, which means that its effect on groundwater movement is small.

The results of radiometric measurements are shown in the Fig. 6 in the form of a curve of total gamma-ray activity eU$_t$ [Ur] smoothed by 3-points-running average and a bar plot of the volume activity of radon ^{222}Rn (VAR) in soil air [kBq.m^{-3}] along the measured profile. Both methods indicate two different geological and soil environments with a lithological boundary around 210–220 m. Due to the shallow depth range of the gamma-ray spectrometry method, there is no direct indication of a deeper vertical boundary confirmed by other geophysical methods at about 165 m of the profile. However, the position of change reflects quite well the observations made in seismic and electric tomography, where near the surface, the basement rocks continue further SE than the fault position at depth.

The soil radon bar plot shows a trend opposite to the total gamma-ray activity curve. The reason is evidently the difference in both the geochemical composition of the geological
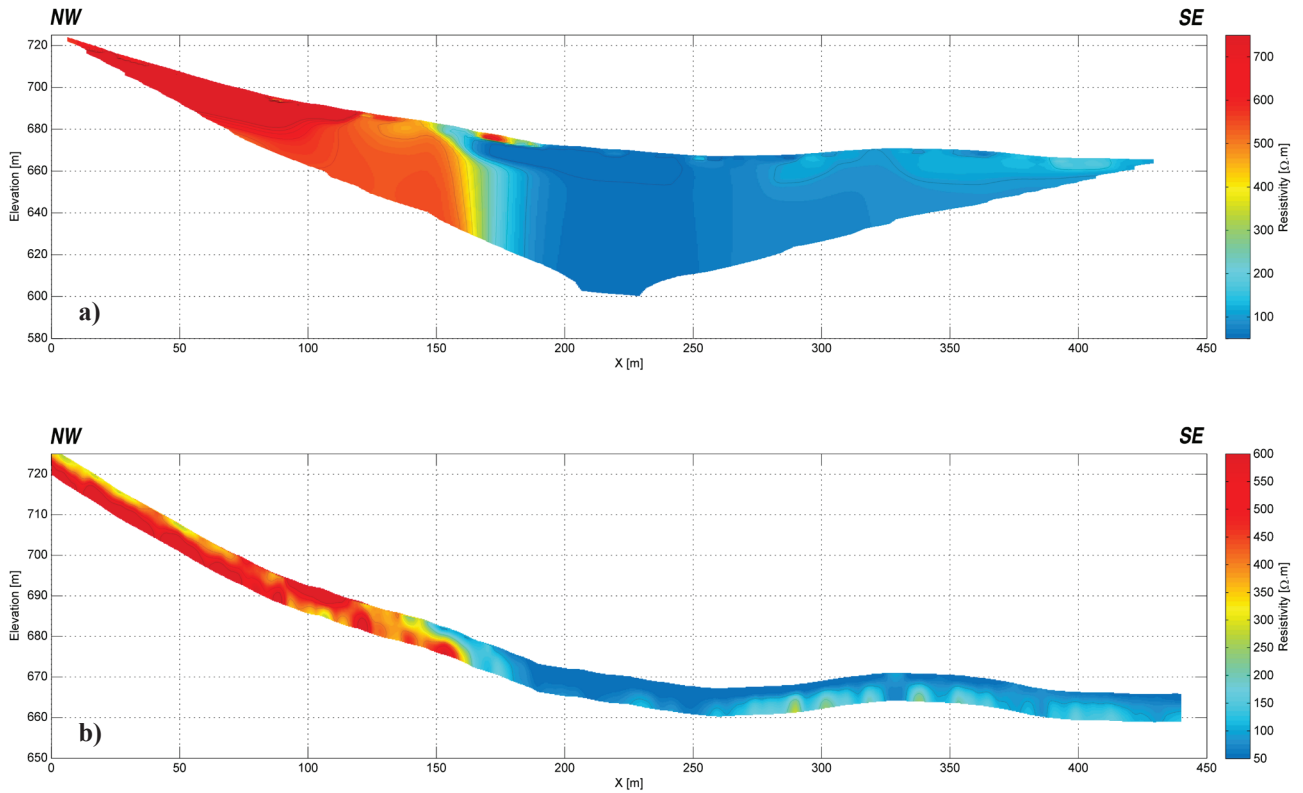
Fig. 4. Resistivity cross-section along the Profile A–A' constructed from electrical resistivity tomography measurement (**a**) and from electromagnetic induction measurement (**b**). The NW block represented by the Tatric crystalline rocks is characterized by higher resistivity values (>400 Ω.m), while the SE block the resistivity of the Neogene sediments is smaller (<200 Ω.m).

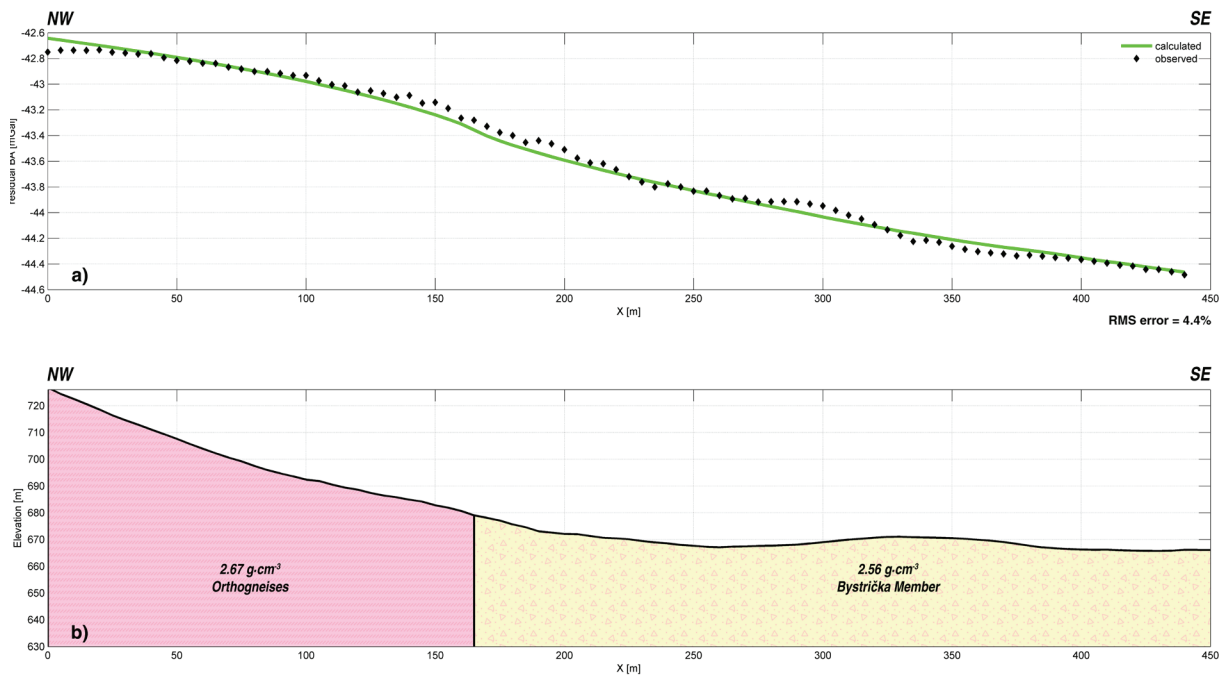

Fig. 5. Density modelling results: **a** — Observed (black diamonds) and calculated (green line) gravity anomalies related to the constructed density model (**b**). Model consists of two density blocks, the NW block has density of 2670 kg.m⁻³ corresponding to the Tatric crystalline complex and the SE block with density of 2560 kg.m⁻³ representing Neogene sediments of the Bystrička Member.
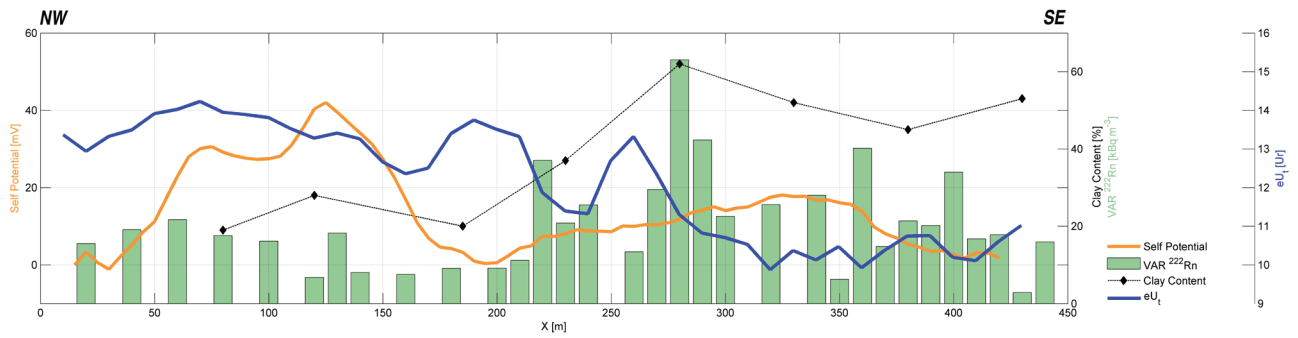
Fig. 6. Self-potential (orange line) and radiometric measurements – in the form of the volume activity of radon ^{222}Rn (VAR) presented as green bars, the total gamma-ray activity eUt [Ur] curve (blue line) and grain analysis results (black line) along the Profile A–A'. The Hradište fault location identified at 165 m along the profile in seismic (Fig. 3) and electric tomography (Fig. 4) is indicated by low VAR values. Lithological boundary from eUt curve is shifted to stations 200–210 m as an effect of downhill erosional transport.
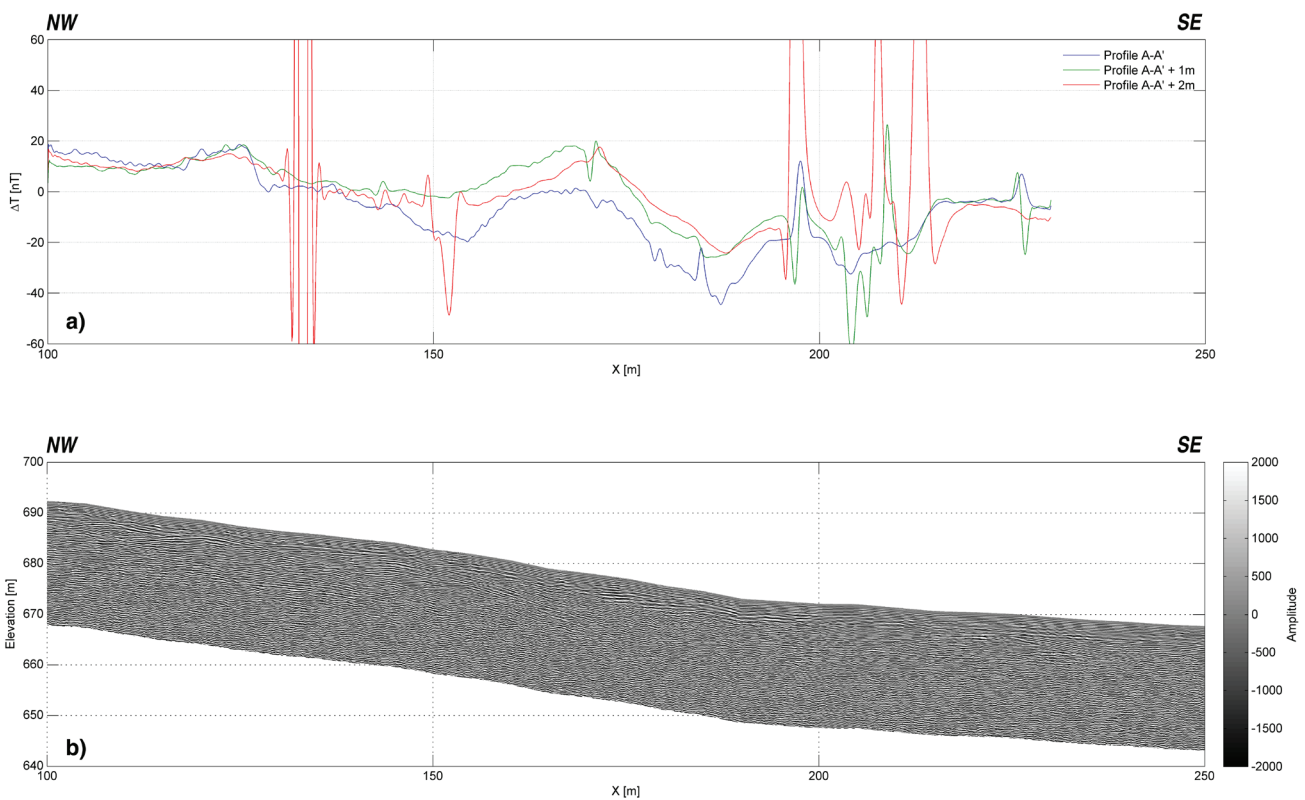

Fig. 7. Results of geomagnetic (**a**) and GPR (**b**) measurements on a selected part of Profile A–A'. The evidence of a vertical contact is not visible in the GPR results, while a low amplitude local maximum recorded between 155 and 185 m along the profile is most likely connected to the fault's presence, but the geomagnetic data are severely distorted by an occurrence of surface iron objects, causing strong local anomalies.

units in contact and their difference in soil gas-permeability. We did grain-size laboratory analysis for eight samples separated 50 m from each other. The results are presented in Fig. 6 (black line) in terms of fine-grained percentage value (clay content) along the line. Table 1 shows the weight and percentage of the fine-grained fraction. Measurements between 140 and 180 m have the lowest values for volume activity of ^{222}Rn in soil air (8 kBq.m^{-3} on average). These small values can probably be explained by the presence of highly permeable

mylonitic material related to fault deformation, allowing easy escape of soil air to the atmosphere.

The evolution of fine-grained (ø<0.063 mm) percentage (clay content) in soil samples along the measured line in Fig. 6 shows that the NW part of the line (0–210/220 m) has lower content of clay particles (average 22 %) in the near-surface horizon than in the SE part (210/220 – 440 m) with an average value of 50 %. This is another confirmation of a contact between the crystalline basement of the Tatric Unit in the NW

part and the Neogene sediments in the SE part of the study line. These values also indicate that near the surface, the contact between the two blocks is found some 30–40 m SE of the contact at depth.

In contrast with the above presented results, where each of the applied method gave insight into the fault system settings, geomagnetics and GPR method were rather unsuccessful. Results from these methods are presented in Fig. 7 for the interesting part of the survey line (100–250 m). The geomagnetic data (Fig. 7a) were measured on three parallel lines along the main profile spaced by 1 m. Unfortunately, their geological interpretation was disabled due to the existence of several surface iron objects, causing local anomalies with amplitudes of several hundred nT. A low amplitude local maximum recorded between 155 and 185 m is most likely connected to presence of the fault, however we believe that the fault could not be identified from geomagnetic data without previous knowledge of fault location obtained from the other geophysical methods used.

The final processed GPR dataset is shown in Fig. 7b. Time-depth conversion was carried out using a constant velocity 0.1 m.ns^{-1}, which was estimated by velocity adaptation of several reflection hyperbolas in the dataset. Though a vertical boundary cannot show up in the reflections, one might expect variations across the contact zone in other parameters such as attenuation or lateral continuity of reflectors. The profile does not show any sign of lateral variations. We suppose that the electromagnetic waves were not able to cross the near-surface weathering zone with clay contents above 20 %.

Discussion

By comparing the results achieved in this work with the results of geophysical measurements carried out on the profiles crossing the Muráň fault zone (Putiška et al. 2012) and on the Dúbrava fault system (Marko et al. 2015; Brixová et al. 2018, 2019) it was found that not all geophysical methods have the same use in finding and mapping faults in the Western Carpathians. It has been found that shallow seismic, ERT, and Dipole electromagnetic profiling have shown the best results. Measuring and displaying resistivity appears to be a robust and reliable method for determining the fault zone (Putiška et al. 2012). Direct indication of the fault zone by soil radon emanometry, whether increased (the Muráň fault zone, Putiška et al. 2012) or decreased (the Hradište border fault) values of soil radon volumetric activity is possible. But compared to geoelectric and seismic measurements, its results are more ambiguous. Gravimetry, gamma-ray spectrometry, magnetometry show their advantages mainly in the identification of the boundaries of rock units and geological objects separated by the fault zone, which are characterized by different values of physical properties. Georadar measurements provided the weakest results so far. On the contrary if the faults are represented by conductive zones (Brixová et al. 2019) then the very low frequency method shows good results.

Table 1: Results of laboratory soil granularity analysis (for dry soil sample).

Station [m]	Total weight [g]	Fraction ø>0.063 mm		Fraction ø<0.063 mm	
		[g]	[%]	[g]	[%]
80	1470.48	1195.52	81	274.96	19
120	1623.20	1174.33	72	448.87	28
185	1861.93	1487.03	80	374.89	20
230	1111.58	703.79	63	407.79	37
280	1562.45	578.93	37	983.52	62
330	569.95	275.30	48	294.65	52
380	1440.98	794.13	55	646.85	45
430	1555.47	727.93	47	827.54	53

From previous experience we can conclude that the choice of suitable geophysical methods for exploring fault systems not only in the Western Carpathians but also in other mountains will always depend on the real geological structure and physical parameters of the rock environment, which are separated by the investigated fault. Therefore, we recommend, as far as possible, to use the widest possible complex of different geophysical measurements. The combination of independent geophysical results allows us to reliably identify subsurface fault zones.

Conclusions

Detailed analysis of the geophysical measurements and their interpretations indicate that the Hradište border fault zone represents a sharp velocity, resistivity and density contrast located at 165 m from the origin of the profile. This zone is almost vertical and characterized by a decrease of the velocity from 3.0 km.s^{-1} to 2.2 km.s^{-1} (Fig. 3) and of electric resistivity from 500 to 150 Ω.m (Fig. 4) and by a maximum horizontal gravity (Fig. 5). Based on SP and radiometric measurements there is no clear indication of this fault zone at the stations around 165 m. This vertical anomalous zone separates two different materials: the orthogneisses of the Tatric crystalline complex belonging to the Malá Fatra Mts. in the NW with high seismic velocities (3.0 km.s^{-1}), resistivity (500 Ω.m), density (2670 kg.m^{-3}), total gamma-ray activity (11 to 14 Ur) and low volume activity of radon (15 kBq.m^{-3} on average) in contrast to the sediments of the Bystrička Member of the Turiec Basin in the SE with low values of seismic velocity (<2.5 km.s^{-1}), resistivity (<200 Ω.m), density (2560 kg.m^{-3}), total gamma-ray activity (10 to 11 Ur) and higher volume activity of radon (25 kBq.m^{-3} on average). These two blocks are covered by a thin surface layer (with a thickness varying in an interval of 5 to 12 m), characterized by rather low seismic velocities 0.5–1.5 km.s^{-1}.

The results obtained along the profile clearly demonstrated that the near-surface geophysics methods are suitable and useful for determining subsurface faults and that it is preferable to take advantage of more than one method. Thus, the presented results helped to discover the hidden position of the Hradište fault and extend our knowledge of this border fault. Our

detailed multidisciplinary geophysical research on this important tectonic fault zone can serve as a case study for geophysical research on faults in the Western Carpathians and other similar orogens.

References

Bielik M., Krajňák M., Makarenko I., Legostaeva O., Starostenko V., Bošanský M., Grinč M. & Hók J. 2013: 3D gravity interpretation of the pre-Tertiary basement in the intramontane depressions of the Western Carpathians: a case study from the Turiec Basin. *Geol. Carpath.* 64, 5, 399–408. https://doi.org/10.2478/geoca-2013-0027

Brixová B., Mosná A. & Mojzeš A. 2018: Geophysical research of the Western Carpathians faults – Sološnica (case study). *Exploration Geophysics, Remote Sensing and Environment* XXV.2, 12–19. https://doi.org/10.26345/EGRSE-012-18-202

Brixová B., Mosná A., Mojzeš A., Rozimant K. & Marko F. 2019: New results in geophysical research of the Western Carpathians faults in the Sološnica area (the Malé Karpaty Mts., Slovakia). In: Proceedings of abstracts of 37th Czech–Polish–Slovak Symposium and 28th Conference "OVA´19", Rožnov p. Radhoštěm, Czech Republic, 9–10.

Corry C.E., DeMoully G.T. & Gerety M.T. 1983: Field procedure manual for self-potential surveys. Australia: *Zone Engineering Research Organization*.

Dubey C.S., Shukla D.P., Singh R.P., Sharma M., Ningthoujam R.S. & Bhola A.M. 2012: Present activity and seismogenic potential of Himalayan sub-parallel thrust faults in Delhi: Inferences from remote sensing, GPR, gravity data and seismicity. *Near Surface Geophysics* 10, 369–380. https://doi.org/10.3997/1873-0604.2012006

EMTOMO 2015: EM4Soil-v2.03 – a program for 1D laterally constrained inversion. In: EMTOMO (Ed.).

Fendek M., Gašparik J., Gross P., Janči J., Kohút M., Kráľ J., Kullmanová A., Planderová E., Raková J., Rakús M., Snopková P., Tuba Ľ., Vass D. & Vozárová A. 1990: Technical report on geothermal borehole ZGT-3 Turiec in Martin and prognostic resources of geothermal energy in the area of Martin. *Open file report — Geofond*, Bratislava, 1–86 (in Slovak).

Fusán O., Biely A., Ibrmajer J., Plančár J. & Rozložník L. 1987: Basement of Tertiary of the Inner West Carpathians. *D. Štúr Geol. Inst.*, Bratislava, 1–103.

Giammanco S., Immé G., Mangano G., Morelli D. & Neri M. 2009: Comparison between different methodologies for detecting radon in soil along an active fault: The case of the Pernicana fault system, Mt. Etna (Italy). *Applied Radiation and Isotopes* 67, 178–185. https://doi.org/10.1016/j.apradiso.2008.09.007

Guerra M. & Lombardi S. 2001: Soil-gas method for tracing neotectonic faults in clay basins: the Pisticci field (Southern Italy). *Tectonophysics* 339, 511–522. https://doi.org/10.1016/S0040-1951(01)00072-5

Hók J., Kováč M., Rakús M., Kováč P., Nagy A., Kováčová-Slamková M., Sitár V. & Šujan M. 1998: Geological and tectonic evolution of the Turiec depression in the Neogene. *Slovak Geol. Mag.* 4, 3, 165–176.

Hrdlička M., Mayerová M., Nehybka J., Novotný M., Sedlák J., Huňáček F. & Viščor J. 1983: Reinterpretation of Profile K-III. *Open file report — Geofond*, Bratislava, 1–56 (in Czech).

Keller G.V. & Frischknecht F.C. 1996: Electrical methods in geophysical prospecting. *Pergamon Press*, Inc., 1–513.

Kilényi E. & Šefara J. 1989: Pre-Tertiary basement contour map of the Carpathian Basin beneath Austria, Czechoslovakia and Hungary. *Eötvös Lóránd Geophys. Inst.*, Budapest, Hungary.

Klinger F.L., Orts D., Gimenez M., Folguera A. & Martinez P. 2016: Multiple geophysical methods used to examine neotectonic structures in the western foothills of the Sierra de El Maitén (Argentina), North Patagonian Andes. *Near Surface Geophysics* 14, 255–262. https://doi.org/10.3997/1873-2016003

Kováč M., Hók J., Minár J., Vojtko R., Bielik M., Pipík R., Rakús M., Kráľ J., Šujan M. & Králiková S. 2011: Neogene and Quaternary development of the Turiec Basin and landscape in its catchment: a tentative mass balance model. *Geol. Carpath.* 62, 4, 361–379. https://doi.org/10.2478/v10096-011-0027-6

Linsser H. 1967: Investigation of Tectonic by Gravity Detailing. *Geophysical Prospecting* 15, 480–515.

Loke M.H. & Barker R.D. 1996: Rapid least-squares inversion of apparent resistivity pseudosections by a quasi-Newton method. *Geophysical Prospecting* 44, 131–152.

Marko F., Dyda M., Gajdoš V., Rozimant K. & Mojzeš A. 2015: Field mapping of buried faults – a new approach applied in the Western Carpathians. *Geol. Quarterly* 59, 1, 35–46. https://doi.org/10.7306/gq.1199

McNeill J.D. 1980: Electromagnetic terrain conductivity measurement at low conduction numbers. *Geonics*, 1–15.

Monteiro Santos F.A., Triantafilis J., Taylor R.S., Holladay S. & Bruzgulis K.E. 2010: Inversion of conductivity profiles from EM using full solution and a 1-D laterally constrained algorithm. *Journal of Environmental and Engineering Geophysics* 15, 163–174. https://doi.org/10.2113/JEEG15.3.163

Neal A. 2004: Ground penetrating radar and its use in sedimentology: principles, problems and progress. *Earth-Sci. Rev.* 66, 261–330. https://doi.org/10.1016/j.earscirev.2004.01.004

Nemčok M. & Lexa J. 1990: Evolution of the Basin and Range structure around the Žiar Mts, range. *Geol. Zbor. Geol. Carpath.* 41, 3, 229–258.

Panáček A., Šefara J., Filo M., Stránska M., Filo M., Kubeš P., Halmešová S., Novák J., Muška P., Steiner A., Gašparík J., Gorek J., Miko O., Rakús M., Havrila M., Polák M., Bujnovský A., Halouzka R., Pivko D., Medo S., Vrábľová D., Rosová M. & Kandrík M. 1991: Map of geophysical indications and interpretations. *Open file report — Geofond*, Bratislava, 1–86 (in Slovak).

Polák M. (Ed.), Potfaj M., Filo I., Broska I., Kohút M., Mello J., Bezák V., Teťák F., Gross P., Biely A., Rakús M., Hók J., Vozár J., Nagy A. & Maglay J. 2008: General geological map of the Slovak republic 1:200 000. Map sheet 26 – Žilina. *Ministry of the Environment of Slovak Republic, Geological Survey of Slovak Republic*, Bratislava.

Pucci S., Civico R., Villani F., Ricci T., Delcher E., Finizola A., Sapia V., De Martini P.M., Pantosti D., Barde-Cabusson S., Brothelande E., Gusset R., Mezon C., Orefice S., Peltier A., Poret M., Torres L. & Suski B. 2016: Deep electrical resistivity tomography along the tectonically active Middle Aterno Valley (2009 L'Aquila earthquake area, central Italy). *Geophys. J. Int.* 207, 2, 967–982. https://doi.org/10.1093/gji/ggw308

Putiška R., Dostál I., Mojzeš A., Gajdoš V., Rozimant K. & Vojtko R. 2012: The resisitivity image of the Muráň fault zone (Central Western Carpathians) obtained by electrical resistivity tomography. *Geol. Carpath.* 63, 3, 233–239. https://doi.org/10.2478/v10096-012-0017-3

Sandmeier K.J. 2014: Reflex-W – Manual (online document). http://www.sandmeier-geo.de/download.html

Sasaki Y. 1989: Two–dimensional joint inversion of magnetotelluric and dipole–dipole resistivity data. *Geophysics* 54, 254–262. https://doi.org/10.1190/1.1442649

Sasaki Y. 2001: Full 3-D inversion of electromagnetic data on PC. *Journal of Applied Geophysics* 46, 45–54. https://doi.org/10.1016/S0926-9851(00)00038-0

Šefara J., Bielik M., Bodnár J., Čížek P., Filo M., Gnojek I., Grecula P., Halmešová S., Husák Ľ., Janoštík B., Král M., Kubeš P., Kucharič Ľ., Kurkin M., Leško B., Mikuška J., Muška P., Obernauer D., Pospíšil L., Putiš M., Šutora A. & Velich R. l987: Structure-tectonic map of the Inner Western Carpathians for the prognoses of the ore deposits – geophysical interpretations. Explanation to the collection of the maps. *Open file report — Geophysics* Brno, *Enterprise* Bratislava, 1–267 (in Slovak).

Sheley D., Crosby T., Zhou M., Giacoma J., Yu J., He R. & Schuster G.T. 2003: 2-D seismic trenching of colluvial wedges and faults. *Tectonophysics* 368, 51–69. https://doi.org/10.1016/S0040-1951(03)00150-1

Singh S., Dinesh K.S., Sunil D. & Surjit S.R. 2006: Geological significance of soil gas radon: A case study of Nurpur area, district Kangra, Himachal Pradesh, India. *Radiation Measurements* 41, 482–485. https://doi.org/10.1016/j.radmeas.2005.10.009

Sládek J. 2010: The morphotectonic field reflection in geomorphological network in the Turčianska Kotlina basin and its surroundings. *PhD. Thesis, Comenius University*, Bratislava, 1–120.

Slater L. & Niemi T.M. 2003: Ground-penetrating radar investigation of active faults along the Dead Sea Transform and implications for seismic hazards within the city of Aqaba, Jordan. *Tectonophysics* 368, 33–50. https://doi.org/10.1016/S0040-1951(03)00149-5

Slovak Technical Norm STN 72 1001, 2010: Soil and rock classification (in Slovak).

Triantafilis J. & Monteiro Santos F.A. 2013: Electromagnetic conductivity imaging (EMCI) of soil using a DUALEM-421 and inversion modeling software (EM4Soil). *Geoderma* 211–212, 28–38. https://doi.org/10.1016/j.geoderma.2013.06.001

Triantafilis J., Odeh I. O.A., Minasny B. & McBratney A.B. 2003: Elucidation of physiographic and hydrogeological features of the lower Namoi valley using fuzzy k-means classification of EM34 data. *Environmental Modeling & Software* 18, 667–680. https://doi.org/10.1016/S1364-8152(03)00053-7

Vajda P. & J. Pánisová 2005: Practical comparison of formulae for computing normal gravity at the observation point with emphasis on the territory of Slovakia. *Contr. Geophys. Geod.* 35, 2, 173–188.

Villani F., Pucci S., Civico R., De Martini P.M., Nicolosi I., Caracciolo F.D., Carluccio R., Di Giulio G., Vassallo M., Smedile A. & Pantosti D. 2015: Imaging the structural style of an active normal fault through multidisciplinary geophysical investigation: A case study from the MW 6.1, 2009 L'Aquila earthquake region (central Italy). *Geophys. J. Int.* 200, 3, 1676–1691. https://doi.org/10.1093/gji/ggu462

Vojtko R., Beták J., Hók J., Marko F., Gajdoš V., Rozimant K. & Mojzeš A. 2011: Pliocene to Quaternary tectonics in the Horná Nitra Depression (Western Carpathians). *Geol. Carpath.* 62, 4, 381–393. https://doi.org/10.2478/v10096-011-0028-5

Zelt C.A. & Smith R.B. 1992: Seismic traveltime inversion for 2-D crustal velocity structure. *Geophys. J. Int.* 108, 16–34. https://doi.org/10.1111/j.1365-246X.1992.tb00836.x